

# First observation of laser-beam interaction in a dipole magnet

Jiawei Yan<sup>1,2</sup>, Nanshun Huang<sup>1,2</sup>, Zheng Qi<sup>3</sup>, Kaiqing Zhang<sup>3</sup>, Kaishang Zhou<sup>3</sup>, Tao Liu<sup>3</sup>, Si Chen<sup>3</sup>, Chao Feng<sup>3</sup>, Chunlei Li<sup>3</sup>, Lie Feng<sup>3</sup>, Taihe Lan<sup>3</sup>, Wenyan Zhang<sup>3</sup>, Xingtao Wang<sup>3</sup>, Xuan Li<sup>3</sup>, Zenggong Jiang<sup>3</sup>, Baoliang Wang<sup>3</sup>, Zhen Wang<sup>3</sup>, Duan Gu<sup>3</sup>, Meng Zhang<sup>3</sup>, Haixiao Deng<sup>3,\*</sup>, Qiang Gu<sup>3</sup>, Yongbin Leng<sup>3</sup>, Lixin Yin<sup>3</sup>, Bo Liu<sup>3</sup>, Dong Wang<sup>3</sup>, and Zhentang Zhao<sup>3,+</sup>

<sup>1</sup>Shanghai Institute of Applied Physics, Chinese Academy of Sciences, Shanghai 201800, China

<sup>2</sup>University of Chinese Academy of Sciences, Beijing 100049, China

<sup>3</sup>Shanghai Advanced Research Institute, Chinese Academy of Sciences, Shanghai 201210, China

\*denghaixiao@zjlab.org.cn

+zhaozhentang@sinap.ac.cn

## ABSTRACT

As a new-generation light source, free-electron lasers (FELs) provide high-brightness X-ray pulses at the angstrom–femtosecond space and time scales. The fundamental physics behind the FEL is the interaction between an electromagnetic wave and a relativistic electron beam in an undulator, which consists of hundreds or thousands of dipole magnets with an alternating magnetic field. Here, we report the first observation of the laser-beam interaction in a pure dipole magnetic field, in which the electron beam energy modulation with 40-keV amplitude and 266-nm period is measured. We also demonstrate that such an energy modulation can be used to launch a seeded FEL, that is, lasing at the sixth harmonic of the seed laser in a high-gain harmonic generation scheme.

## Introduction

A charged particle radiating energy in the form of an electromagnetic wave when it is accelerated is the basic principle behind modern accelerator-based light sources. Among such sources, synchrotron radiation and free-electron lasers (FELs) have played key roles in numerous scientific fields by providing high-brightness electromagnetic waves over a wide spectral range. X-ray FELs<sup>1</sup>, which are considered to be the next generation of light sources, are capable of providing femtosecond X-ray pulses with a peak brightness ten orders of magnitude higher than the third-generation synchrotron light sources. Compared to synchrotron radiation, the amplification of the FEL pulse comes from the strong and continuous interaction between an electromagnetic wave and a relativistic electron beam in a periodic lattice of alternating dipole magnetic fields, known as an undulator.

In an FEL process, the interaction between the electromagnetic wave and electrons causes energy modulation of the electron beam. The energy modulation evolves into longitudinal density modulation on the scale of the FEL wavelength, referred to as bunching. The bunching contributes to the FEL power growth, and the amplified FEL power further enhances and speeds up the bunching. This positive feedback loop leads to an exponential growth of the FEL power in a high-gain FEL. Owing to the existence of such a feedback mechanism, the undulator spontaneous emission can be used as an initial seed to drive the FEL amplification at short wavelengths, a mechanism known as self-amplified spontaneous emission, which is the baseline principle of most X-ray FELs worldwide<sup>2-6</sup>.

In addition to the FEL power amplification, the presence of energy modulation caused by laser-beam interaction also enables modern X-ray FEL facilities to achieve better performance and various unique characteristics<sup>7</sup>. Seeded FELs employ an external laser to trigger the FEL frequency up-conversion, making them ideal for providing stable, fully coherent X-rays<sup>8</sup>. Typically, in a seeded FEL scheme, such as high-gain harmonic generation (HG<sup>9</sup>), the energy of the electron beam is periodically modulated by a seed laser. A dispersive magnetic chicane is used to transform the purely sinusoidal energy modulation into density bunching that contains high harmonic components. Then, the bunched electron beams are used to produce highly coherent FEL pulses at the preferred harmonics. More advanced seeded FEL schemes are being developed to improve the frequency multiplication efficiency<sup>10-12</sup>. In addition, a laser heater<sup>13,14</sup> is normally placed before the bunch compressor in the linac section of an X-ray FEL facility, where an external laser is employed to interact with the electron beam, thereby increasing the uncorrelated beam energy spread and thus suppressing the microbunching instability induced by the

effects of the longitudinal space charge and coherent synchrotron radiation. Furthermore, the laser-beam interaction is proposed to widely manipulate and rearrange the electron distributions and then generate attosecond coherent pulses<sup>15-18</sup>, mode-locked X-ray pulse sequences<sup>19,20</sup>, and X-rays with orbital angular momentum<sup>21,22</sup> to satisfy different scientific requirements.

An electron beam moving along a straight line cannot interact with an electromagnetic wave in free space. The beam needs a curved trajectory to achieve efficient interaction with the electromagnetic field. The energy change of the electron with a horizontal motion in an electromagnetic field is given by  $mc^2 \frac{d\gamma}{dt} = ev_x E_x$ , where  $\gamma mc^2$  is the electron energy,  $E_x$  is the horizontal electric field of the electromagnetic wave, and  $v_x$  is the horizontal velocity of the electron. Currently, all the interactions between the electromagnetic wave and the electron beam are accomplished in the undulator. In general, one undulator period is treated as the standard unit in FEL physics; for example, the well-known FEL equations<sup>23</sup> and well-benchmarked codes GENESIS<sup>24</sup> and GINGER<sup>25</sup> are based on the undulator-period-averaged mode. However, one undulator period consists of a series of dipole magnetic fields. The interaction between the electromagnetic wave and the electron beam has already taken place when the electron beam passes through each of the basic components of the undulator, namely a dipole magnetic field, which is the fundamental process of the FEL interaction<sup>26</sup>. To the best of our knowledge, all experimentally observed interactions between the electromagnetic wave and the electron beam are the cumulative effect of passing through one full undulator, i.e., tens to hundreds or even thousands of dipole magnetic fields. In this work, we artificially designed and conducted an experiment at the Shanghai soft X-ray FEL (SXFEL) test facility<sup>27</sup> to study the interaction between an electromagnetic wave and an electron beam in a pure dipole magnetic field. In the experiment, the energy modulation of the electron beam induced by an ultraviolet laser in a dipole magnet was observed and measured. Furthermore, the feasibility of seeded FEL lasing using such energy modulation was also demonstrated.

## Results

The schematic layout of the experiment is shown in Fig. 1. An 800-MeV electron beam with a bunch length of  $\sim 1$  ps (full width at half maximum (FWHM)) and a bunch charge of 600 pC was sent into the first chicane, which consisted of four dipole magnets with a length of 0.3 m. A 266-nm external laser with a pulse length of 160 fs (FWHM) was expected to interact with the electron beam at the first dipole magnet, and a metallic baffle was placed in the middle of the chicane to draw the laser out so that the electron beam did not interact with the laser at the fourth dipole magnet. Once the beam energy modulation is formed in the first dipole magnet, it is converted to density bunching when the electron beam passes through the remaining part of the entire chicane. This means that, in this experiment, both energy modulation and density bunching were accomplished in the first chicane. To ensure a sufficiently strong electric field in the interaction, the laser waist was tuned to near the first dipole magnet. The radius of the laser at the first dipole was  $\sim 200 \mu\text{m}$ . In addition to the intensity and profile of the laser, the energy exchange obtained from the laser-beam interaction also depends on the electron beam trajectory in the laser field. Therefore, the interaction in the dipole magnet was correlated with the strength of the magnetic field. Because the magnetic field of the dipole magnet also determines the dispersion strength of the chicane, the energy modulation and density bunching were mutually coupled in the chicane.

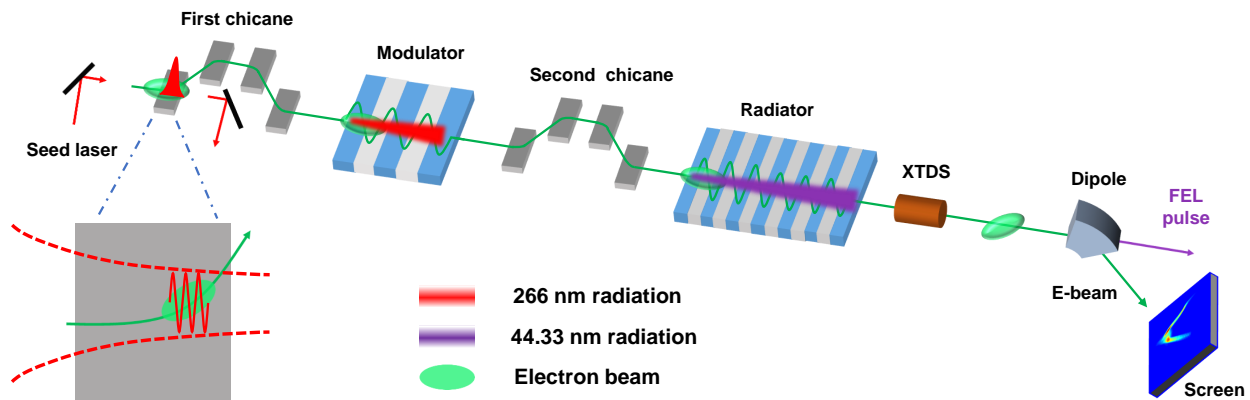


**Figure 1.** Schematic layout of the experiment. An 800-MeV electron beam is sent to the first chicane and interacts with a 266-nm seed laser in the first dipole magnet. Energy modulation and density modulation are performed simultaneously in the first chicane. In the modulator, an electron beam is used to generate coherent radiation at the fundamental wavelength, which also enhances the energy modulation. The radiator is used to produce FEL pulses at the sixth harmonic of the seed laser.

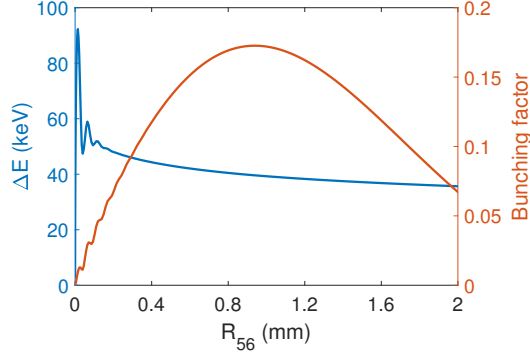


**Figure 2.** Three-dimensional tracking of the laser-beam interaction. Plotted are the energy modulation amplitude of the electron beam and bunching factor as a function of the dispersion strength of the first magnetic chicane.

We first used a three-dimensional tracking algorithm based on electrodynamics<sup>26</sup> to analyze the laser-beam interaction in the dipole magnet. In the simulation, all parameters were determined according to the experimental settings. The initial slice energy spread of the electron beam was set to 30 keV according to the measurements in the normal operation of the SXFEL. The peak power of the laser was set to 220 MW. The density modulation of the electron beam was quantified by the bunching factor. As presented in Fig. 2, the simulation reveals the relationship between the value of  $R_{56}$  of the chicane and the obtained energy modulation amplitude as well as the bunching factor at the fundamental wavelength after passing through the chicane. When  $R_{56}$  is set to 0.01 mm, an energy modulation amplitude of 92 keV can be obtained. However, owing to constraints from the actual chicane configuration, the dipole magnetic field of the first chicane is adjustable from 0.03 to 0.12 T, corresponding to  $R_{56}$  values of 0.11 to 1.7 mm. In this range, the energy modulation changes slowly from 52 to 36 keV, and a bunching factor of  $>0.1$  can be obtained at the fundamental wavelength. In theory, an electron beam with such a strong bunching factor can be used to produce significant coherent radiation.

In the experiment, the electron beam was sent to interact with the external laser in the first dipole magnet of the first chicane. The laser pulse energy was set to be its maximum, i.e., 38.10  $\mu\text{J}$ . The  $R_{56}$  value of the first chicane was set at  $\sim 0.9$  mm according to the three-dimensional tracking result. To observe the changes in the electron beam after the interaction, the gaps of the modulator and the radiator were fully opened. Here, we used an X-band transverse deflecting structure (XTDS) and a dipole magnet at the end of the undulator section to measure the longitudinal phase space of the electron beam. When the laser pulse was successfully synchronized with the electron beam, significant changes in the phase space were observed in the electron beam, and the location of these changes shifted with the adjustment of the laser timing synchronization. Fig. 3(a) shows a typical longitudinal phase space of the electron beam with changes in the central part.

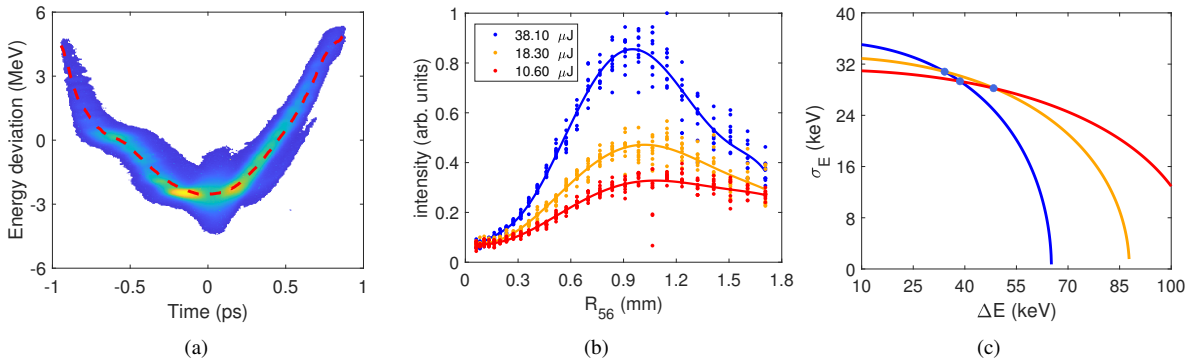


**Figure 3.** Performance of the laser-beam interaction in the dipole magnet. (a) Longitudinal phase space of the electron beam after the interaction. The red dashed line represents the central energy of the electron beam. Beam head is on the left. (b) Measured coherent radiation intensity and fitted curves after the electron beam passes through the first chicane under different laser pulse energies. The coherent radiation intensity is recorded by a photodiode when the dispersion strength of the first chicane is scanned. (c) Relationship between the energy modulation amplitude induced by the 38.10  $\mu\text{J}$  seed laser and the initial slice energy spread.

We further measured the energy modulation amplitude induced in the dipole magnetic field through the generation of coherent radiation<sup>28</sup>. In the measurement, the following modulator with a length of 1.5 m and a period of 80 mm was set to be resonant at 266 nm and thus to generate coherent radiation at the fundamental wavelength of the external laser. Next, we scanned the dispersion strength of the first chicane to determine the optimal dispersion strength that maximizes the intensity of the coherent radiation. As presented in the three-dimensional simulation results, the energy modulation amplitude varies very slowly in the scanning range of  $R_{56}$ . Therefore, we considered that the energy modulation amplitude was fixed under a specific external laser. According to the measurement method, a numerical relationship between the energy modulation amplitude and the average slice energy spread can be obtained through the optimal dispersion strength of the chicane. Consequently, multiple numerical relationships need to be obtained by varying the laser pulse energy, and their intersections were treated as the measurement result. In addition to 38.10  $\mu\text{J}$ , two other laser pulse energies of 18.3 and 10.6  $\mu\text{J}$  were also used to interact with the electron beam. The measured intensities of the coherent radiation and the fitted curves based on the measurement under the three laser pulse energies are shown in Fig. 3(b). Three optimal  $R_{56}$  values of 0.95, 1.02, and 1.08 mm were obtained under the three different laser pulse energies. As displayed in Fig. 3(c), according to the three optimal  $R_{56}$  values, three numerical relationships are modeled, where all the energy modulation amplitudes are scaled to that obtained by the laser pulse energy of 38.10  $\mu\text{J}$ . The average of the three intersections was regarded as the measurement result. The measured slice energy spread was 28 keV, which is consistent with the measurement results under normal FEL operation. The measured energy modulation amplitude induced by the external laser with 266-nm wavelength and 38.10- $\mu\text{J}$  pulse energy in a dipole magnet of 0.3 m was 40 keV, which reasonably agrees with the simulation result.

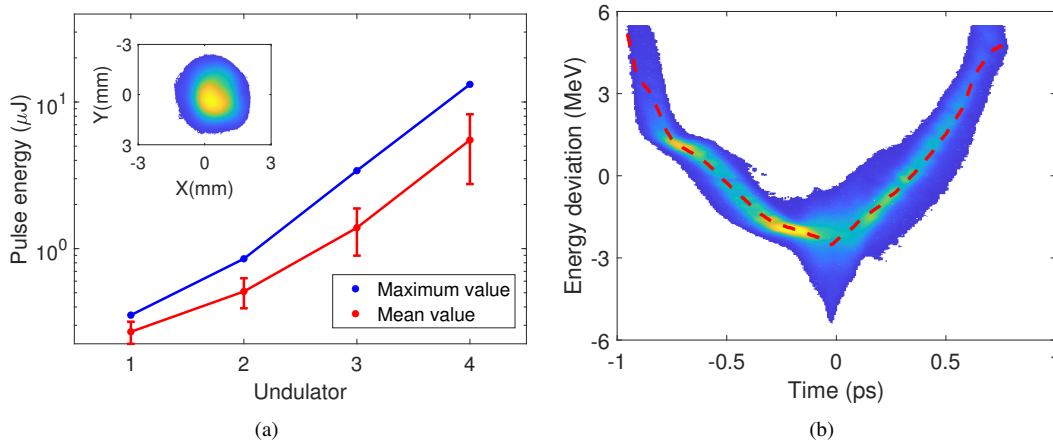


**Figure 4.** Performance of the FEL lasing at the sixth harmonic of the seed laser. (a) Gain curve and typical transverse profile of the FEL pulse at 44.33 nm. The red and blue points represent the average pulse energy and maximum pulse energy at the end of various undulator segments, respectively. The FEL pulse energy was measured by a calibrated photodiode at the end of the undulator section. The error bars represent the root-mean-square intensity fluctuations. The inset displays one typical transverse profile of the FEL pulse. (b) Typical longitudinal phase space of the electron beam at the exit of the radiator.

We have demonstrated and measured the laser–beam interaction in a dipole magnetic field. The obtained energy modulation is a factor of 1.4 greater than the slice energy spread in our case, which is one order of magnitude less than that in a modulator undulator. The dipole magnet and laser pulse coexist in many parts of an FEL facility. Because the introduced energy modulation is considerable, the laser–beam interaction in the dipole magnetic field cannot be ignored and needs to be carefully considered in the design and operation of the FEL, especially in cases where the ultimate output performances are pursued. In addition, the energy modulation induced in a dipole magnet has many potential applications. Because a laser-induced energy spread of  $\sim 20$  keV is sufficient to suppress microbunching instabilities, a chicane without an undulator could be a future option for the laser heater. Moreover, even larger energy modulation would be obtained by using a laser with a higher peak power or an optimized dipole magnet, thus generating a fully coherent FEL by exploiting energy modulation is a more straightforward application.

In this work, we explored the feasibility of using the energy modulation obtained in the dipole magnet for FEL lasing at the sixth harmonic of the seed laser. Limited by existing hardware, it is difficult to increase the peak power of the seed laser or change the dipole magnet. The energy modulation amplitude of a factor of 1.4 greater than the slice energy spread is difficult to use for lasing at the sixth harmonics directly; consequently, the self-modulation method<sup>29</sup> was employed to further enhance

the energy modulation. In the experiment, the pulse energy of the seed laser was kept at  $38.10 \mu\text{J}$ . The dispersion strength of the first chicane was set at the optimal value to maximize the intensity of the coherent radiation in the modulator. As a result, the electron beam was modulated by the coherent radiation generated by itself, and the energy modulation was enhanced. Thereafter, we sent the electron beam to the radiator, which was composed of four undulator segments with a length of 3 m and a period of 40 mm. Initially, only the first undulator segment was used for coherent radiation generation at the sixth harmonic of the seed laser. Then, the dispersion strength of the second chicane was scanned to maximize the coherent radiation intensity. According to the optimal dispersion strength of 0.16 mm obtained from the scanning and the previously obtained slice energy spread of 28 keV, we estimated an energy modulation of 253 keV after self-modulation. The results indicated that the energy modulation amplitude was increased sixfold through self-modulation.

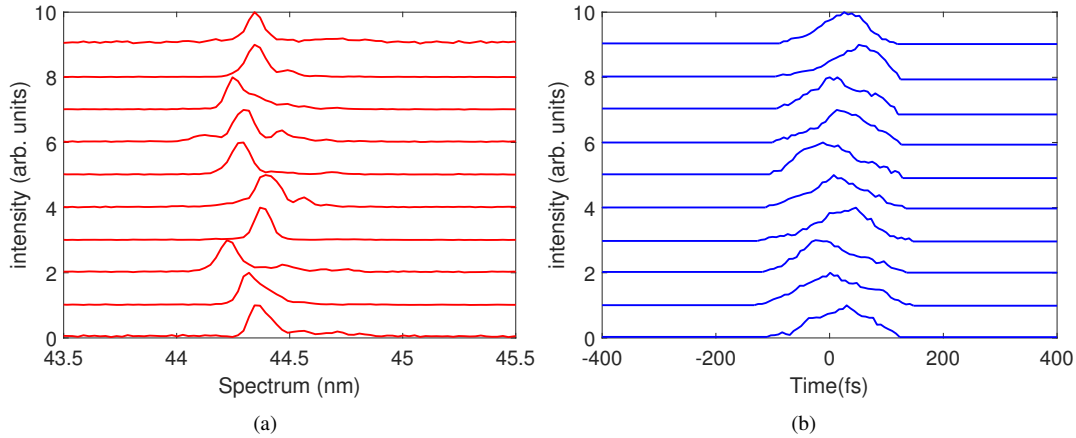


**Figure 5.** Spectra and reconstructed temporal profiles of 44.33-nm FEL pulses. (a) Ten typical spectra measured by the spectrometer after the radiator. (b) Power profiles of ten typical FEL pulses reconstructed by using the XTDS system.

Combined with the enhanced energy modulation after the modulator, the second chicane and the radiator were used for HGHG lasing at 44.33 nm. The dispersion strength of the second chicane was maintained at the optimal value. Other undulator segments of the radiator were used to further amplify the 44.33-nm radiation. Fig. 4(a) presents the maximum and average pulse energies of the FEL pulse after each undulator segment and one typical transverse profile of the FEL pulse. At the end of the radiator, FEL pulses with an average pulse energy of  $5.5 \mu\text{J}$  and a root-mean-square energy jitter of  $2.7 \mu\text{J}$  were obtained. One typical longitudinal phase of the electron beam after the radiator is shown in Fig. 4(b). A drop in the centroid kinetic energy can be observed at the central part of the electron beam. The spectra of the FEL pulses were measured using a spectrometer with a resolution of 0.05 nm. The average FWHM bandwidth over 60 consecutive shots was  $1.7 \times 10^{-3}$ . Fig. 5(a) shows ten typical measured spectra. In addition, we reconstructed the temporal profile of the FEL pulse according to the change in the centroid energy of the electron beam<sup>30</sup>. Ten typical temporal profiles of FEL pulses are presented in Fig. 5(b).

## Discussion

In summary, for the first time, we have demonstrated and measured the interaction between a laser and relativistic electrons in a pure dipole magnet. A 266-nm laser was used to interact with an 800-MeV electron beam in a dipole magnet. The measured energy modulation amplitude was 40 keV, which is consistent with the theoretical tracking results. This experiment intuitively reveals a fundamental step in the FEL process and thus contributes to a deeper understanding of FEL physics. Moreover, as an example, we have shown that the energy modulation obtained in a dipole magnet can be used for lasing at the sixth harmonic of the seed laser in an HGHG setup.

The results presented here open up a new direction for the interaction between lasers and relativistic electron beams. The use of laser-beam interaction in a dipole magnet to introduce energy modulation for suppressing microbunching instability or tailoring FEL pulse properties makes the FEL facility more compact and cost-effective. Using a seed laser with a peak power of hundreds of gigawatts, it is possible to directly obtain an energy modulation amplitude on the order of MeV for seeded FELs without additional self-modulation. Furthermore, based on this scheme, the complex manipulation of the electron beam in echo-enabled harmonic generation can be accomplished in two magnetic chicanes, which greatly simplifies the configuration of the facility. Because the laser-beam interaction in a dipole magnet does not have a specific resonance condition, it is well tolerant of energy jitter and chirp and is promising for electron beams from plasma wakefield based accelerators.

From another perspective, our results highlight that the existence of laser-beam interaction in a dipole magnetic field may lead to considerable energy modulation. As more and more laser systems are used in FEL facilities, this effect should be taken into account in many FEL operations. In particular, using an external laser to modulate an electron beam normally requires the use of a chicane for laser injection, which means that the laser inevitably interacts with the fourth dipole magnet of the chicane. For FEL schemes that utilize laser modulation for attosecond pulse generation, an external laser with high intensity is often employed. In such cases, the laser-beam interaction in the laser injection chicane, or even in the correctors, would significantly perturb the initial beam quality, which may degrade the final achieved FEL performance. Therefore, the energy modulation occurring in the dipole magnets should be reasonably matched to the modulation in the undulator.

## Method

### Machine setup

The experiment was conducted at the SXFEL test facility. An electron beam with a beam energy of  $\sim 130$  MeV, a bunch charge of  $\sim 600$  pC, a bunch length (FWHM) of  $\sim 10$  ps, and a transverse emittance of  $\sim 1$   $\mu$ mrads was generated in the photoinjector. In the following linac section, the electron beam was further boosted by four S-band and six C-band accelerating structures to  $\sim 800$  MeV. The bunch length of the electron beam was compressed to  $\sim 1$  ps using a magnetic chicane. The seed laser pulses were generated by a commercial Ti: sapphire laser system that provides 800-nm laser pulses with an energy of up to  $\sim 3$  mJ. A third-harmonic generation was used to convert the laser pulses to 266 nm ( $\sim 130$  fs).

### Diagnostics

At the exit of the undulator section, an XTDS was employed in conjunction with an electron beam energy spectrometer to measure the longitudinal phase space of the electron beam and the power profile of the FEL pulse. Two 0.65-m-long X-band deflecting structures with a total deflecting voltage of 8 MV were used to streak the electron beam horizontally. After a drift section, a 1.5-m-long dipole magnet vertically dispersed the electrons of different energies. A yttrium aluminum garnet crystal screen was used to capture the electron beam downstream of the dipole magnet. The final temporal resolution obtained was  $\sim 15$  fs, and the energy resolution was  $\sim 30$  keV. The FEL spectra were measured using a dedicated VUV spectrometer (McPherson, Model 234/302) with spectral coverage from 40 to 200 nm. The intensity of the FEL radiation was diagnosed by using the photodiodes at the end of the undulator section.

## References

1. Pellegrini, C., Marinelli, A. & Reiche, S. The physics of x-ray free-electron lasers. *Rev. Mod. Phys.* **88**, 015006, DOI: <https://doi.org/10.1103/RevModPhys.88.015006> (2016).
2. Emma, P. *et al.* First lasing and operation of an angstrom-wavelength free-electron laser. *NATURE PHOTONICS* **4**, 641–647, DOI: <https://doi.org/10.1038/NPHOTON.2010.176> (2010).
3. Ishikawa, T. *et al.* A compact X-ray free-electron laser emitting in the sub-angstrom region. *NATURE PHOTONICS* **6**, 540–544, DOI: <https://doi.org/10.1038/nphoton.2012.141> (2012).
4. Decking, W. *et al.* A MHz-repetition-rate hard X-ray free-electron laser driven by a superconducting linear accelerator (vol 14, pg 6311, 2020). *NATURE PHOTONICS* **14**, 650+, DOI: <https://doi.org/10.1038/s41566-020-0680-3> (2020).
5. Kang, H.-S. *et al.* Hard X-ray free-electron laser with femtosecond-scale timing jitter. *NATURE PHOTONICS* **11**, 708+, DOI: <https://doi.org/10.1038/s41566-017-0029-8> (2017).
6. Prat, E. *et al.* A compact and cost-effective hard x-ray free-electron laser driven by a high-brightness and low-energy electron beam. *Nat. Photonics* **14**, 1–7, DOI: <https://doi.org/10.1038/s41566-020-00712-8> (2020).
7. Hemsing, E., Stupakov, G., Xiang, D. & Zholents, A. Beam by design: Laser manipulation of electrons in modern accelerators. *Rev. Mod. Phys.* **86**, 897–941, DOI: <https://doi.org/10.1103/RevModPhys.86.897> (2014).
8. Feng, C. & Deng, H.-X. Review of fully coherent free-electron lasers. *NUCLEAR SCIENCE AND TECHNIQUES* **29**, DOI: <https://doi.org/10.1007/s41365-018-0490-1> (2018).
9. Yu, L. H. Generation of Intense UV Radiation by Subharmonically Seeded Single-pass Free-Electron Lasers. *Phys. Rev. A* **44**, 5178–5193, DOI: <https://doi.org/10.1103/PhysRevA.44.5178> (1991).
10. Stupakov, G. Using the beam-echo effect for generation of short-wavelength radiation. *Phys. Rev. Lett.* **102**, 074801, DOI: <https://doi.org/10.1103/PhysRevLett.102.074801> (2009).
11. Deng, H. & Feng, C. Using off-resonance laser modulation for beam-energy-spread cooling in generation of short-wavelength radiation. *Phys. Rev. Lett.* **111**, 084801, DOI: <https://doi.org/10.1103/PhysRevLett.111.084801> (2013).

12. Stupakov, G. Frequency multiplication using coherent radiation of a “snake” beam. *Phys. Rev. ST Accel. Beams* **16**, 010702, DOI: <https://doi.org/10.1103/PhysRevSTAB.16.010702> (2013).
13. Huang, Z. *et al.* Suppression of microbunching instability in the linac coherent light source. *Phys. Rev. ST Accel. Beams* **7**, 074401, DOI: <https://doi.org/10.1103/PhysRevSTAB.7.074401> (2004).
14. Tang, J. *et al.* Laguerre-gaussian mode laser heater for microbunching instability suppression in free-electron lasers. *Phys. Rev. Lett.* **124**, 134801, DOI: <https://doi.org/10.1103/PhysRevLett.124.134801> (2020).
15. Zholents, A. A. & Fawley, W. M. Proposal for intense attosecond radiation from an x-ray free-electron laser. *Phys. Rev. Lett.* **92**, 224801, DOI: <https://doi.org/10.1103/PhysRevLett.92.224801> (2004).
16. Zholents, A. A. Method of an enhanced self-amplified spontaneous emission for x-ray free electron lasers. *Phys. Rev. ST Accel. Beams* **8**, 040701, DOI: <https://doi.org/10.1103/PhysRevSTAB.8.040701> (2005).
17. Saldin, E. L., Schneidmiller, E. A. & Yurkov, M. V. Self-amplified spontaneous emission fel with energy-chirped electron beam and its application for generation of attosecond x-ray pulses. *Phys. Rev. ST Accel. Beams* **9**, 050702, DOI: <https://doi.org/10.1103/PhysRevSTAB.9.050702> (2006).
18. Tanaka, T. Proposal for a pulse-compression scheme in x-ray free-electron lasers to generate a multiterawatt, attosecond x-ray pulse. *Phys. Rev. Lett.* **110**, 084801, DOI: <https://doi.org/10.1103/PhysRevLett.110.084801> (2013).
19. Thompson, N. R. & McNeil, B. W. J. Mode locking in a free-electron laser amplifier. *Phys. Rev. Lett.* **100**, 203901, DOI: <https://doi.org/10.1103/PhysRevLett.100.203901> (2008).
20. Kur, E., Dunning, D. J., McNeil, B. W. J., Wurtele, J. & Zholents, A. A. A wide bandwidth free-electron laser with mode locking using current modulation. *New J. Phys.* **13**, 063012, DOI: <https://doi.org/10.1088/1367-2630/13/6/063012> (2011).
21. Hemsing, E. *et al.* Helical electron-beam microbunching by harmonic coupling in a helical undulator. *Phys. Rev. Lett.* **102**, 174801, DOI: <https://doi.org/10.1103/PhysRevLett.102.174801> (2009).
22. Hemsing, E., Marinelli, A. & Rosenzweig, J. B. Generating optical orbital angular momentum in a high-gain free-electron laser at the first harmonic. *Phys. Rev. Lett.* **106**, 164803, DOI: <https://doi.org/10.1103/PhysRevLett.106.164803> (2011).
23. Bonifacio, R., Pellegrini, C. & Narducci, L. Collective instabilities and high-gain regime in a free electron laser. *Opt. Commun.* **50**, 373 – 378, DOI: [https://doi.org/10.1016/0030-4018\(84\)90105-6](https://doi.org/10.1016/0030-4018(84)90105-6) (1984).
24. Reiche, S. Genesis 1.3: a fully 3d time-dependent fel simulation code. *Nucl. Instruments Methods Phys. Res. Sect. A: Accel. Spectrometers, Detect. Assoc. Equip.* **429**, 243 – 248, DOI: [https://doi.org/10.1016/S0168-9002\(99\)00114-X](https://doi.org/10.1016/S0168-9002(99)00114-X) (1999).
25. Fawley, W. M. A user manual for ginger and its post-processor xplotgin. Tech. Rep., Lawrence Berkeley National Lab.(LBNL), Berkeley, CA (United States) (2002).
26. Deng, H., Yan, J., Wang, D. & Dai, Z. Laser-induced energy modulation in a dipole and potential applications for fel. *Nucl. Instruments Methods Phys. Res. Sect. A: Accel. Spectrometers, Detect. Assoc. Equip.* **622**, 508 – 511, DOI: <https://doi.org/10.1016/j.nima.2010.07.064> (2010).
27. Zhao, Z. *et al.* Status of the sxfel facility. *Appl. Sci.* **7**, 607, DOI: <https://doi.org/10.3390/app7060607> (2017).
28. Feng, C. *et al.* Measurement of the average local energy spread of electron beam via coherent harmonic generation. *Phys. Rev. ST Accel. Beams* **14**, 090701, DOI: <https://doi.org/10.1103/PhysRevSTAB.14.090701> (2011).
29. Yan, J. *et al.* Self-amplification of coherent energy modulation in seeded free-electron lasers. Preprint at <https://arxiv.org/abs/2011.01080> (2020).
30. Behrens, C. *et al.* Few-femtosecond time-resolved measurements of X-ray free-electron lasers. *NATURE COMMUNICATIONS* **5**, DOI: <https://doi.org/10.1038/ncomms4762> (2014).

## Data availability

Data supporting the figures and other findings in this manuscript are available from the corresponding authors upon request.

## Acknowledgments

This work was partially supported by the National Key Research and Development Program of China (Grant Numbers 2018YFE0103100 and 2016YFA0401900) and the National Natural Science Foundation of China (Grant Numbers 11935020 and 11775293).

## **Author contributions**

J.W.Y. and H.X.D. proposed, designed, and realized the experiment at the SXFEL test facility. J.W.Y., H.X.D., and Z.T.Z co-wrote the manuscript. All authors contributed to the construction and commissioning of the SXFEL.

## **Competing interests**

The authors declare no competing interests.